

Provably Quantum-Secure Microgrids through Enhanced Quantum Distributed Control

Pouya Babahajiani, *Senior Member, IEEE*, P. Zhang, Ji Liu, *Member, IEEE*, and Tzu-Chieh Wei

Abstract—Distributed control of multi-inverter microgrids has attracted considerable attention as it can achieve the combined goals of flexible plug-and-play architecture guaranteeing frequency and voltage regulation while preserving power sharing among nonidentical distributed energy resources (DERs). However, it turns out that cybersecurity has emerged as a serious concern in distributed control schemes. Inspired by quantum communication developments and their security advantages, this paper devises a scalable quantum distributed controller that can guarantee synchronization, and power sharing among DERs. The key innovation lies in the fact that the new quantum distributed scheme allows for exchanging secret information directly through quantum channels among the participating DERs, making microgrids inherently cybersecure. Case studies on two ac and dc microgrids verify the efficacy of the new quantum distributed control strategy.

Index Terms—Quantum-secure microgrid control, distributed frequency regulation, distributed voltage regulation.

MICROGRIDS have emerged as a promising new paradigm of electricity resiliency which deliver a growing share of the energy [1] and facilitate the penetration of the renewable resources into grid utility. In this spirit, in order to match up with their main characteristics including flexibility and scalability, microgrids are becoming ever more reliant on distributed control frameworks [2], [3], and hence they have become cyber-physical systems that requires complicated network technologies to handle massive utilization of communication and computation devices [4].

On the other hand, while distributed control strategies can enhance microgrids resilience, they may cause cybersecurity challenges since they can be vulnerable to cyber attacks on communication links. Malicious signals from third party agents can drive the microgrid toward inconsistent performance and instability of the whole system [5].

Finding solutions to encounter cybersecurity issues in microgrids with distributed control strategies is an ongoing research [3], [6], [7]. However, the existing solutions may become insecure due to the rapid development of supercomputers and the emergence of quantum computers [8], [9] and so they can make traditional/classical methods obsolete. Utilizing principles

of quantum mechanics, quantum communication offers provable security of communication and is a promising solution to counter such threats [9].

Quantum physics principles give rise to novel capability unachievable with classical transmission media. In these schemes, information is encoded in the particle's quantum state, which cannot be copied, and any attempt to do so can be detected. Therefore, the critical aspect is unconditional information security which is impossible with classical information processing [10]. The key benefit of using quantum-secured information is that the lifetime of the security is "infinite", i.e., it will be secure against any future advance in computation capability [10].

Therefore, quantum communication [11]–[13] has proposed a revolutionary step in secure communication due to its high security of the quantum information, and many models including quantum key distribution (QKD) [14], quantum teleportation [15], discrete-variable quantum secure direct communication [16], [17] and continuous variable quantum secure direct communication [18] have been developed. Based on QKD technology, many different types of quantum communication networks have been proposed [14], [19]. However, these communication networks based on QKD technology only transmit the key, but do not directly transmit information. On the other hand, quantum secure direct communication is a kind of information carrier with quantum state in communication. In this method, secret information is directly transmitted over a secure quantum channel and inspite of QKD schemes, they do not require key distribution and key storage [16].

Recent development in quantum physics suggests the possibility of investigating consensus problems for networks of quantum nodes [20]–[22]. In [22], it is shown that consensus can be obtained for a network of quantum nodes through establishing interactions among them by means of swapping operators, so that the whole network is described by a Lindblad master equation with the Lindblad terms generated by the swapping operators. Lindblad equation [23], [24] is utilized to describe the state evolution of quantum systems which have interactions with environment. Another approach is exploiting the gossip-type interaction between neighboring quantum nodes [20].

The existing approaches, however, are not utilizable for the problem of distributed control in microgrids for two main reasons. First, as we will elaborate more in the following sections, the distributed control problem in microgrids is a distributed tracking problem within which, both possibly time-varying targets and coupling mechanisms exist. Although in [22], the swapping operator is exploited to build an underlying interaction graph and therefore the coupling mechanism for the quantum network, for the zero Hamiltonian case, the network's final state is the average of the initial states, and under the non-zero

This work was supported in part by the US Department of Energy's Office of Electricity under Agreement No. 37533, in part by the US National Science Foundation under Grant Nos. ECCS-2018492, OIA-2134840 and OIA-2040599, and in part by Stony Brook University's Office of the Vice President for Research through a Quantum Information Science and Technology Seed Grant. T.-C. Wei was supported by the National Science Foundation under Grant No. PHY-1915165.

P. Babahajiani, P. Zhang and J. Liu are with the Department of Electrical and Computer Engineering, Stony Brook University, NY 11794, USA (e-mails: pouya.babahajiani, p.zhang, ji.liu@stonybrook.edu).

T.-C. Wei is with C.N. Yang Institute for Theoretical Physics, Stony Brook University, NY 11794-3800, USA (e-mail: tzu-chieh.wei@stonybrook.edu).

Hamiltonian, each qubit tends to the same trajectory related to the network Hamiltonian and initial states of all the nodes. The latter mostly is difficult to derive the explicit trajectory of each qubit [22]. Second, these schemes are valid as long as the corresponding quantum system is not measured, which is necessary as at each time step, the information needs to be extracted (or encoded) from (or into) the quantum nodes, which makes these schemes impractical for realistic distributed control of microgrids.

Inspired by the existing cybersecurity challenges in microgrids with classical distributed control frameworks, in a recent work [25], we devised a quantum distributed control for ac and dc microgrids within which, the information carrier is quantum states and the transmission media is a quantum channel, i.e., information is encoded into quantum states which are directly sent over quantum channels among participating DERs, while the control objectives including power/current sharing and frequency/voltage regulation are guaranteed. In this method, there is an assumption that at each time-step, qubits are (re-)initialized on the first quarter of the equator of the Bloch sphere and therefore the evolution of the qubits at each node on the equator is translated into control signal.

In this paper, we demonstrate, however, that with this assumption, the synchronization might not be achieved if quantum states become mixed over the time steps. Furthermore, it might be possible for a third party agent to find out that information is being encoded into the phase angle of the exchanged qubits. We aim to show that by some modifications and relaxing this assumption, the problem of mixed states can be tackled and also the security of the algorithm can be significantly enhanced such that even if a third party agent can measure the exchanged qubits, the measurement outcomes would be some random values which do not reveal information to the eavesdropper. Consequently, adversaries can not access nor falsify the data exchanged among DERs. The key contribution is therefore a provably quantum-secure distributed control that enables unprecedentedly resilient and cybersecure microgrids.

The rest of the paper is organized as follows. In Section II we formulate the problem by reviewing our recently proposed quantum distributed control in [25] and then pointing out the issues. Section III presents the developed quantum-secure distributed controller (QSDC) together with a numerical example. Section IV is devoted to explain the devised QSDC for ac and dc microgrids. Simulation results are also provided. Section V concludes the paper.

I. PROBLEM FORMULATION

To formulate our problem, we present an overview of the developed quantum distributed controller proposed in [25] followed by a discussion on the issues that can impair the synchronization of the network under this scheme. Fundamental materials from graph theory [34] and quantum systems [29] used throughout the paper can be found in Appendix A.

A. Quantum Distributed Control

Distributed control problems of microgrids can be described as a network of differential equations over a simple, connected

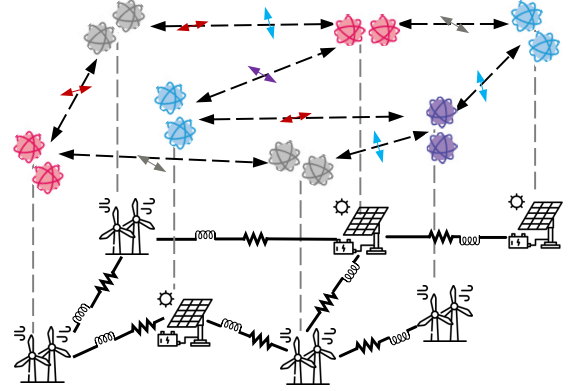


Fig. 1. Coupling of the physical microgrid to the network of quantum controllers - Information is exchanged through quantum communication.

graph $G = (V, E)$ whose node set $V = \{v_1, v_2, \dots, v_n\}$ represents n DERs and edge set E depicts allowable communication among the DERs. These DERs evolve through interactions, according to certain networking scheme and dynamics.

As a representative example, the goal of the distributed frequency control problem in ac microgrids is to regulate the network frequency to a rated value and guarantee active power sharing among the DERs, whose dynamics can be described by

$$\begin{aligned} \omega_i &= \omega^* - n_i P_i + \Phi_i, \\ \dot{\Phi}_i &= f(\Phi_i, P_i, \Phi_j, j \in N_i), \end{aligned} \quad (1)$$

where ω_i represents the frequency at DER_{*i*}, ω^* is a nominal network frequency, P_i is the active power injection at DER_{*i*}, n_i is the droop gain, and the dynamics of Φ_i represents the secondary control variable, which is a function (f) of its current value, P_i , and its neighbors' values Φ_j 's which eventually evolves toward an (weighted) average of its neighbours values Φ_j such that all control variables Φ_i converge to the common value $\Phi_i = \Phi_j = n_i P_i$.

By the same token, the problem of distributed voltage control and power/current sharing in DC microgrids, can be formulated similar to that of Eq. (1), as Eq. (2) which will be discussed more in Section IV:

$$\begin{aligned} V_i^{ref} &= V^* - m_i I_i + \Phi_i, \\ \dot{\Phi}_i &= f(\Phi_i, I_i, \Phi_j, j \in N_i), \end{aligned} \quad (2)$$

where V_i^{ref} is the generated voltage reference, V^* is the nominal dc voltage, m_i is the current droop gain, and I_i is the output current of DER_{*i*}.

In [25], the goal is to construct a network of differential equations, such as those in Eqs. (1) and (2), to control a network of DERs as shown in Fig. 1. There, in contrast to the classical synchronization, quantum bits are what is exchanged among the nodes and the framework is formulated as follows.

- In this framework, each microgrid is equipped with or connected to a quantum computing (QC) device, which prepares a quantum state and then seeks a consensus among all the QCs in a distributed manner. The state of each quantum device can be described by a positive Hermitian density matrix ρ . Since synchronization requires interaction among all quantum devices, it is assumed that each device has access to the (quantum) information of its neighbors. Let $|\psi\rangle = |q_1 q_2 \dots q_n\rangle$ be the

state of the whole quantum network and $\rho = |\psi\rangle\langle\psi|$. The following Lindblad master equation was introduced to construct the network of differential equations (For more information on Markovian master equations in Lindblad form, which is a suitable way to describe the dynamics of a quantum system with interaction with environment, see [26]):

$$\begin{aligned} \dot{\rho}(t) = & \sum_{i=1}^n \left(C_i \rho C_i^\dagger - \frac{1}{2} \{ C_i^\dagger C_i, \rho \} \right) \\ & + \sum_{\{i,j\} \in E} \left(C_{i,j} \rho C_{i,j}^\dagger - \frac{1}{2} \{ C_{i,j}^\dagger C_{i,j}, \rho \} \right). \end{aligned} \quad (3)$$

where C_i and $C_{i,j}$ are unitary jump operators.

In this scheme, the state of each quantum node at each time step is updated as follows:

$$|q_i(t)\rangle = \cos \frac{\pi}{4} |0\rangle + e^{i\phi_i(t)} \sin \frac{\pi}{4} |1\rangle, \quad t \in \{0, 1, 2, \dots\}, \quad (4)$$

which is the general state in polar coordinates set on the xy-plane, where $\phi_i(0) \in (0, \pi/2)$ and each $\phi_i(t)$, $t \geq 1$, is inferred from the averaged measurement outcome at node i .

In Eq. (3), $C_{i,j}$ is the swap operator that specifies the external interaction between quantum computing devices i and j such that

$$\begin{aligned} C_{i,j}(|q_1\rangle \otimes \dots \otimes |q_i\rangle \otimes \dots \otimes |q_j\rangle \otimes \dots \otimes |q_n\rangle) \\ = |q_1\rangle \otimes \dots \otimes |q_j\rangle \otimes \dots \otimes |q_i\rangle \otimes \dots \otimes |q_n\rangle, \end{aligned} \quad (5)$$

and the jump operator, C_i , is defined as

$$C_i = I^{\otimes(i-1)} \otimes R_z(\phi) \otimes I^{\otimes(n-i)}, \quad (6)$$

with $R_z(\phi)$ being the single-qubit rotation-Z operator by an angle ϕ radians around the Z-axis. By definition, the operator C_i acts only on $|q_i\rangle$ without changing the states of other qubits. As can be seen, the jump operators C_i are state dependent and are updated based on the target values $\phi_{i,t}$ and the measured $\phi_i(t)$. Furthermore, as mentioned earlier, at the beginning of each time step, all the qubits are re-initialized as in (4) based on the measurement outcome of the previous step. Therefore, at each time step, the master equation components are updated based on the target values and the obtained measurement signals. Thus, the density matrix at time $t + dt$ can be decomposed into $\rho(t + dt) = \rho(t) + d\rho_t$, where $d\rho(t)$ is defined in (3).

Next, to obtain ϕ_i , the following observables are utilized:

$$A_{1,i} = I^{\otimes(i-1)} \otimes \sigma_x \otimes I^{\otimes(n-i)}, \quad (7)$$

$$A_{2,i} = I^{\otimes(i-1)} \otimes \sigma_y \otimes I^{\otimes(n-i)}. \quad (8)$$

The operator $I^{\otimes(i-1)} \otimes \sigma_{x/y} \otimes I^{\otimes(n-i)}$ acts only on $|q_i\rangle$ where node-wise means, having σ_x and σ_y which are Pauli matrices as observers at each node,

$$\sigma_x = \begin{pmatrix} 0 & 1 \\ 1 & 0 \end{pmatrix}, \quad \sigma_y = \begin{pmatrix} 0 & -i \\ i & 0 \end{pmatrix}. \quad (9)$$

The expectation value of an observable A in a state, represented by a density matrix ρ , is given by $\langle A \rangle = \text{tr}(\rho A)$ [27]. For a general one qubit state ρ_i , $\text{tr}(\rho_i \sigma_x) = r_i \sin \theta_i \cos \phi_i$, $\text{tr}(\rho_i \sigma_y) = r_i \sin \theta_i \sin \phi_i$ and $\text{tr}(\rho_i \sigma_z) = r_i \cos \theta_i$ where r_i is the size of the state vector i . Generally, Lindblad equation results in states becoming more mixed; however, we only let the system evolve in a short time and re-initialize the system

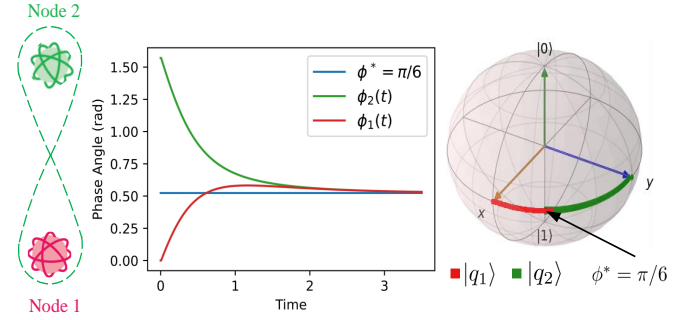


Fig. 2. Exponential synchronization of the phase angles to the target phase $\phi^* = \pi/6$ - (Left side) Connected communication formed by the swap operator - (Right side) Bloch sphere representation shows the trajectories traversed by the qubits along the time.

in a product of pure qubit states. Therefore, we can consider $r = 1$ and $\theta = \pi/2$ and hence

$$\text{tr}(\rho \sigma_x) = \cos \phi_i, \quad \text{tr}(\rho \sigma_y) = \sin \phi_i. \quad (10)$$

which are equivalent to $\text{tr}(\rho A_{1,i}) = \cos \phi_i$ and $\text{tr}(\rho A_{2,i}) = \sin \phi_i$, respectively. Note that $\frac{d}{dt} \langle A \rangle = \frac{d}{dt} \text{tr}(\rho A) = \text{tr}(\dot{\rho} A)$. Hence, it can be readily obtained that, $\frac{d}{dt} \arctan\left(\frac{\text{tr}(\rho A_{2,i})}{\text{tr}(\rho A_{1,i})}\right)$ gives the dynamic of ϕ_i , or the synchronization rule, as follows:

$$\dot{\phi}_i = \sin(\phi_{t,i} - \phi_i) + \sum_{j=1}^n a_{i,j} \sin(\phi_j - \phi_i). \quad (11)$$

where $a_{i,j} = 1$ if $C_{ij} \neq \mathbf{0}$ and $a_{i,j} = 0$ otherwise. ■

It is worth noting that both $\text{tr}(\rho A_{1,i})$ and $\text{tr}(\rho A_{2,i})$ are used in (16) to find the trajectory that ϕ_i traverses along the time; however, either $\arccos(\text{tr}(\rho \sigma_x))$ or $\arcsin(\text{tr}(\rho \sigma_y))$ gives ϕ_i .

As mentioned, at each time-step, qubits are (re-)initialized on the equator of the Bloch sphere and hence, remain on the equator along the process. Fig. (2) shows a numerical example of two qubits (utilizing open source software QuTiP [31]) with the initial states $|q_1\rangle = \frac{1}{\sqrt{2}}[1, 1]^T$ (node 1) and $|q_2\rangle = \frac{1}{\sqrt{2}}[1, i]^T$ (node 2) that get synchronized to the target $\phi^* = \pi/6$ while they remain on the equator along the time.

B. The Problem

There are two issues with the framework just described. First, in case qubits become mixed, neither $\arccos(\text{tr}(\rho \sigma_x))$ nor $\arcsin(\text{tr}(\rho \sigma_y))$ gives ϕ_i and synchronization would not be attained even if θ_i remains $\pi/2$ since, $\arccos(\text{tr}(\rho \sigma_x)) = \arccos(r_i \cos \phi_i) \neq \phi_i$ and Eq. (11) is no longer valid. For instance, Fig. (3) shows how for the two qubits example in Fig. (2), synchronization would be violated if $|q_2\rangle$ slightly becomes mixed at some random steps after the master equation evolution. Second, if the eavesdropper does not know the basis, she can figure out the angle ϕ_i if she has a lot number of qubits and performs state tomography [30] to determine the basis and the angle ϕ_i , allows her to perform false data injection and hence destabilize the microgrid.

In the next section, we demonstrate that by some modifications and relaxing the assumption of (re-)initializing qubits on the equator of Bloch sphere, the security of the algorithm can be significantly enhanced such that even if a third party agent can measure the exchanged qubits, the measurement outcomes would be some random values which do not reveal information to the eavesdropper. Furthermore, even if the states

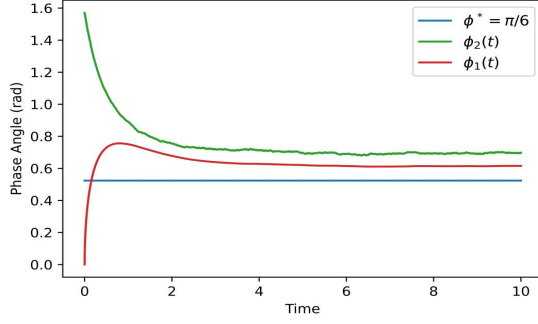


Fig. 3. Violation of synchronization when $|q_2\rangle$ becomes mixed at some steps after the master equation evolution.

become mixed after the master equation evolution, or the (re-)initialization produces mixed states, the synchronization rule remains valid.

II. QUANTUM-SECURE DISTRIBUTED CONTROL

In our developed scheme, the state of each quantum node at each time step is prepared as follows

$$|q_i(t)\rangle = \cos \frac{\theta_i(t)}{2} |0\rangle + e^{i\phi_i(t)} \sin \frac{\theta_i(t)}{2} |1\rangle, \quad t \in \{0, 1, 2, \dots\}, \quad (12)$$

which is the general state in polar coordinates set on the surface of the Bloch sphere, where $0 < \theta_i(t) < \pi$ is a random value and $\phi_i(0) \in (0, \pi/2)$.

Theorem 1. Consider the master equation (3). Let each $\phi_i(t)$, $t \geq 1$, be the averaged measurement outcome at node i , utilizing the observables (7) and (8), such that $\phi_i = \arctan\left(\frac{\text{tr}(\rho A_{2,i})}{\text{tr}(\rho A_{1,i})}\right)$. Then, we have the following:

- 1) The dynamic of ϕ_i can be written as

$$\dot{\phi}_i = \sin(\phi_{t,i} - \phi_i) + \sum_{j=1}^n a_{i,j} \frac{r_j \sin \theta_j}{r_i \sin \theta_i} \sin(\phi_j - \phi_i); \quad (13)$$

- 2) The synchronization rule in 1) remains valid even if the (re-)initialization produces mixed states, or states become mixed after master equation evolution;
- 3) The random angle θ_i randomizes the state and hence on average (over θ_i) the state appears to be random to a third party who measures the exchanged qubits among the quantum nodes.

Proof. As mentioned, for the observables $A_{1,i}$ and $A_{2,i}$, we have the following expectation values:

$$\begin{aligned} \text{tr}(\rho A_{1,i}) &= r_i \sin \theta_i \cos \phi_i, \\ \text{tr}(\rho A_{2,i}) &= r_i \sin \theta_i \sin \phi_i. \end{aligned} \quad (14)$$

Considering (3) and that $\frac{d}{dt}\langle A \rangle = \text{tr}(\dot{\rho}A)$, we can obtain the synchronization rule as follows:

$$\begin{aligned} \text{tr}(\dot{\rho}A_{1,i}) &= r_i \cos \phi_{t,i} \sin \theta_i - r_i \cos \phi_i \sin \theta_i + \\ &\quad \sum_{j=1}^n a_{i,j} (r_j \cos \phi_j \sin \theta_j - r_i \cos \phi_i \sin \theta_i), \\ \text{tr}(\dot{\rho}A_{2,i}) &= r_i \sin \phi_{t,i} \sin \theta_i - r_i \sin \phi_i \sin \theta_i + \\ &\quad \sum_{j=1}^n a_{i,j} (r_j \sin \phi_j \sin \theta_j - r_i \sin \phi_i \sin \theta_i), \end{aligned} \quad (15)$$

where $a_{i,j} = 1$ if $C_{ij} \neq \mathbf{0}$ and $a_{i,j} = 0$ otherwise. Utilizing (14) and (15), the dynamic of ϕ_i can be found as follows:

$$\begin{aligned} \dot{\phi}_i &= \frac{d}{dt} \arctan\left(\frac{\text{tr}(\rho A_{2,i})}{\text{tr}(\rho A_{1,i})}\right) \\ &= \frac{\text{tr}(\dot{\rho}A_{2,i})\text{tr}(\rho A_{1,i}) - \text{tr}(\dot{\rho}A_{1,i})\text{tr}(\rho A_{2,i})}{r_i^2 \sin^2 \theta_i \sin^2 \phi_i + r_i^2 \sin^2 \theta_i \cos^2 \phi_i} \\ &= \frac{1}{r_i^2 \sin^2 \theta_i} \left[\left(r_i \sin \phi_{t,i} \sin \theta_i - r_i \sin \phi_i \sin \theta_i \right. \right. \\ &\quad \left. \left. + \sum_{j=1}^n a_{i,j} (r_j \sin \phi_j \sin \theta_j - r_i \sin \phi_i \sin \theta_i) \right) r_i \cos \phi_i \sin \theta_i \right. \\ &\quad \left. - \left(r_i \cos \phi_{t,i} \sin \theta_i - r_i \cos \phi_i \sin \theta_i + \right. \right. \\ &\quad \left. \left. \sum_{j=1}^n a_{i,j} (r_j \cos \phi_j \sin \theta_j - r_i \cos \phi_i \sin \theta_i) \right) r_i \sin \phi_i \sin \theta_i \right] \\ &= \sin \phi_{t,i} \cos \phi_i - \cos \phi_{t,i} \sin \phi_i + \\ &\quad \sum_{j=1}^n a_{i,j} \frac{r_j \sin \theta_j}{r_i \sin \theta_i} (\sin \phi_j \cos \phi_i - \cos \phi_j \sin \phi_i) \\ &= \sin(\phi_{t,i} - \phi_i) + \sum_{j=1}^n a_{i,j} \frac{r_j \sin \theta_j}{r_i \sin \theta_i} \sin(\phi_j - \phi_i). \end{aligned} \quad (16)$$

As stated, $0 < \theta_i < \pi$ and hence, $(r_j \sin \theta_j)/(r_i \sin \theta_i) > 0$ and so $a_{i,j} \frac{r_j \sin \theta_j}{r_i \sin \theta_i} \geq 0$. Therefore, (16) can be rewritten as

$$\dot{\phi}_i = \sin(\phi_{t,i} - \phi_i) + \sum_{j=1}^n a'_{i,j} \sin(\phi_j - \phi_i), \quad (17)$$

where $a'_{i,j} = a_{i,j} \frac{r_j \sin \theta_j}{r_i \sin \theta_i} > 0$ if $C_{ij} \neq \mathbf{0}$ and $a'_{i,j} = 0$ otherwise. In Appendix B, it is shown that how the pinning term $\sin(\phi_{t,i} - \phi_i)$ forces the phase ϕ_i to stick at the value $\phi_{t,i}$ and the coupling mechanism $\sum_{j=1}^n a'_{i,j} \sin(\phi_j - \phi_i)$ helps to synchronize the entire system and all the nodes will synchronize to the pinner $\phi_{t,i}$ exponentially fast.

The above analysis leads to the following critical property of the proposed quantum-secure distributed control:

- 1) With this scheme, the additional random angle θ_i randomizes the state and hence on average (over θ_i) the state appears to be random, i.e., maximally mixed $I/2$. Then, the eavesdropper cannot figure out the correct 0/1 basis and consequently, the information is being encoded into ϕ_i .
- 2) (16) shows that the scheme works even if the (re-)initialization produces mixed states, or states become mixed along the master equation evolution.

This completes the proof. \square

Considering (14), even if ϕ_i does not change, changing θ_i impacts the expectation values $\text{tr}(\rho A_{1,i})$ and $\text{tr}(\rho A_{2,i})$. Therefore, as shown in (16), both $\text{tr}(\rho A_{1,i})$ and $\text{tr}(\rho A_{2,i})$ are required to find the trajectory traversed by ϕ_i along the time. However, measuring a qubit results in demolishing that quantum state. Hence, to obtain the both expectations at each node, at each time step, two identical qubits will be prepared according to Eq. (12) which will experience the same Master equation evolution. Afterwards, expectation value of σ_x is measured for

one of the qubits and expectation of σ_y for its identical twin. The

Algorithm 1: Quantum-Secured Distributed Control

- 1 At each node, initialize a pair of identical qubits as a point on the surface of the first quarter of the Bloch Sphere, i.e., $0 < \phi_i(0) < \pi/2$ and $0 < \theta_i(t) < \pi$, using Eq. (4) for each adjacent node
 - 2 Transmit quantum information throughout the network such that each quantum node receives a pair of identical qubits from each one of its adjacent nodes
 - 3 At each node, update the rotation-Z (R_z) operator's argument based on the pinner ($\phi_{t,i}$) and the current value of the phase angle ϕ_i
 - 4 Evolve the master Eq. (3) for one time step δt by means of the swapping and rotation-Z operators
 - 5 Measure the expectation value of the σ_x operator for one of the qubits and σ_y for its identical twin. Repeating this multiple times and averaging gives the $r_i \sin \theta_i \cos \phi_i$ and $r_i \sin \theta_i \sin \phi_i$, respectively. On classical hardware at each node, compute $\arctan\left(\frac{\langle \sigma_y \rangle}{\langle \sigma_x \rangle}\right)$ to obtain the phase angle ϕ_i
 - 6 Re-initialize the state of each quantum node according to Eq. (4) and based on the measurement outcomes at step 5
 - 7 Go back to step 2
-

basic outline of the algorithm is summarized in **Algorithm 1**.

Numerical Example. In this example, in addition to synchronization, we illustrate that, how choosing random variables for θ_i results in an unprecedentedly secured distributed control framework. We consider a network composed of three quantum nodes with the following initial states:

$$\begin{aligned} |q_1\rangle &= \cos \frac{1.96}{2} |0\rangle + \sin \frac{1.96}{2} |1\rangle, \\ |q_2\rangle &= \cos \frac{1.49}{2} |0\rangle + e^{\frac{\pi}{8}i} \sin \frac{1.49}{2} |1\rangle, \\ |q_3\rangle &= \cos \frac{2.07}{2} |0\rangle + e^{\frac{\pi}{2}i} \sin \frac{2.07}{2} |1\rangle. \end{aligned}$$

Here, the target is $\phi^* = \frac{\pi}{3}$. The three qubits interact through swapping operators $C_{1,2}$, $C_{2,3}$ and $C_{1,3}$, forming a connected interaction graph as shown in Fig. 4a. We consider the state of the whole quantum network as $\rho = |q_1 q_2 q_3\rangle \langle q_1 q_2 q_3|$. As an illustrative example, the swapping operator $C_{1,2}$ would be as follows:

$$C_{1,2} = \begin{pmatrix} 1 & 0 & 0 & 0 \\ 0 & 0 & 1 & 0 \\ 0 & 1 & 0 & 0 \\ 0 & 0 & 0 & 1 \end{pmatrix} \otimes \begin{pmatrix} 1 & 0 \\ 0 & 1 \end{pmatrix} \quad (18)$$

such that,

$$\begin{aligned} C_{1,2} |q_1(t)q_2(t)q_3(t)\rangle \langle q_1(t)q_2(t)q_3(t)| C_{1,2}^\dagger \\ - |q_2(t)q_1(t)q_3(t)\rangle \langle q_2(t)q_1(t)q_3(t)| = [\mathbf{0}]_{8 \times 8} \end{aligned} \quad (19)$$

The trajectories of ϕ_1 , ϕ_2 and ϕ_3 , i.e. ϕ angles of $|q_1\rangle$, $|q_2\rangle$ and $|q_3\rangle$ respectively, are sketched in Fig. 4b utilizing the Python-based open source software QuTiP [31]. As illustrated, all the three phase angles converge to ϕ^* . Therefore, the final state of each quantum node is the state $[\cos \frac{\theta_i(t)}{2}, e^{\frac{\pi}{2}i} \sin \frac{\theta_i(t)}{2}]^T$ where, $0 < \theta_i(t) < \pi$ is a random value.

As depicted in Fig. 4d, even if the eavesdropper is able to measure the x, y and z components of the exchanged qubits, the measurement outcomes would be some random values which don't reveal meaningful information to the eavesdropper.

To better illustrate that how randomizing θ increases the security of the scheme, a single qubit measurement experiment is provided in the following (Fig. 5). In this numerical example first, it is shown that how measuring the probabilities of the 0/1 basis of the qubit can give the ϕ angle, when qubit is initialized on the equator of the Bloch sphere and there are enough copies of it. Suppose the qubit is initialized as follows:

$$|q\rangle = \cos \frac{\pi}{4} |0\rangle + e^{\frac{\pi}{6}i} \sin \frac{\pi}{4} |1\rangle.$$

It can be readily obtained that the X, Y and Z components of the qubit can be found through measuring the Z basis of the circuits 1, 2 and 3, respectively, where Z, H (Hadamard gate) and S^\dagger are defined as follows:

$$Z = \begin{pmatrix} 1 & 0 \\ 0 & -1 \end{pmatrix}, H = \frac{1}{\sqrt{2}} \begin{pmatrix} 1 & 1 \\ 1 & -1 \end{pmatrix}, S^\dagger = \begin{pmatrix} 1 & 0 \\ 0 & -i \end{pmatrix}.$$

As can be seen, the ϕ angle of the qubit can be found through measuring the probabilities of finding the qubit in 0/1 basis:

$$\cos^{-1}(|\langle 0|q\rangle|^2 - |\langle 1|q\rangle|^2) = \cos^{-1}(0.935 - 0.065) = \frac{\pi}{6}.$$

Hence, if an eavesdropper has access to enough copies of the quantum state, she can figure out ϕ and therefore, the exchanged secret information. Now, we show how by using superposition of qubits, we can significantly enhance the security of the scheme. As mentioned, for a general single qubit, the expectation value of σ_x (which can be obtained by measuring the Z basis of the circuit (2) and subtracting the probabilities) equals to $\langle \sigma_x \rangle = r \sin \theta \cos \phi$, and since the qubit is initialized as a pure state on the equator of the Bloch sphere, $r = 1$ and $\theta = \pi/2$. But when the angle θ is randomized such that:

$$|q\rangle = \cos \frac{\theta}{4} |0\rangle + e^{\frac{\pi}{6}i} \sin \frac{\theta}{4} |1\rangle, \theta \in (0, \pi)$$

$\langle \sigma_x \rangle \neq \cos \phi$ and hence, the probabilities of finding the qubit in 0/1 basis do not give information about the X component, and consequently the encoded information. Fig. (6) shows the probabilities with the circuit (2) which is the average over 2000 shots when random θ is used at each shot. As it is evident, $\cos^{-1}(0.809 - 0.191) \neq \frac{\pi}{6}$, and from Eve's point of view, exchanged qubits are alternating between $|0\rangle$ and $|1\rangle$ basis with no meaningful pattern, which is also demonstrated in Fig. 4d.

III. QUANTUM-SECURED DISTRIBUTED CONTROLLER FOR AC AND DC MICROGRIDS

A. AC Microgrids

Droop control is a local DER control which is used to regulate the DER's frequency ω_i through local measurement of the active power injection at DER_{*i*} as follows

$$\omega_i = \omega^* - n_i P_i \quad (20)$$

where ω^* is a nominal network frequency, P_i is the measured active power injection at DER_{*i*} and n_i is the gain of the droop coefficient. The secondary control is then utilized to restore the operating frequency to the rated value ω^* . Our

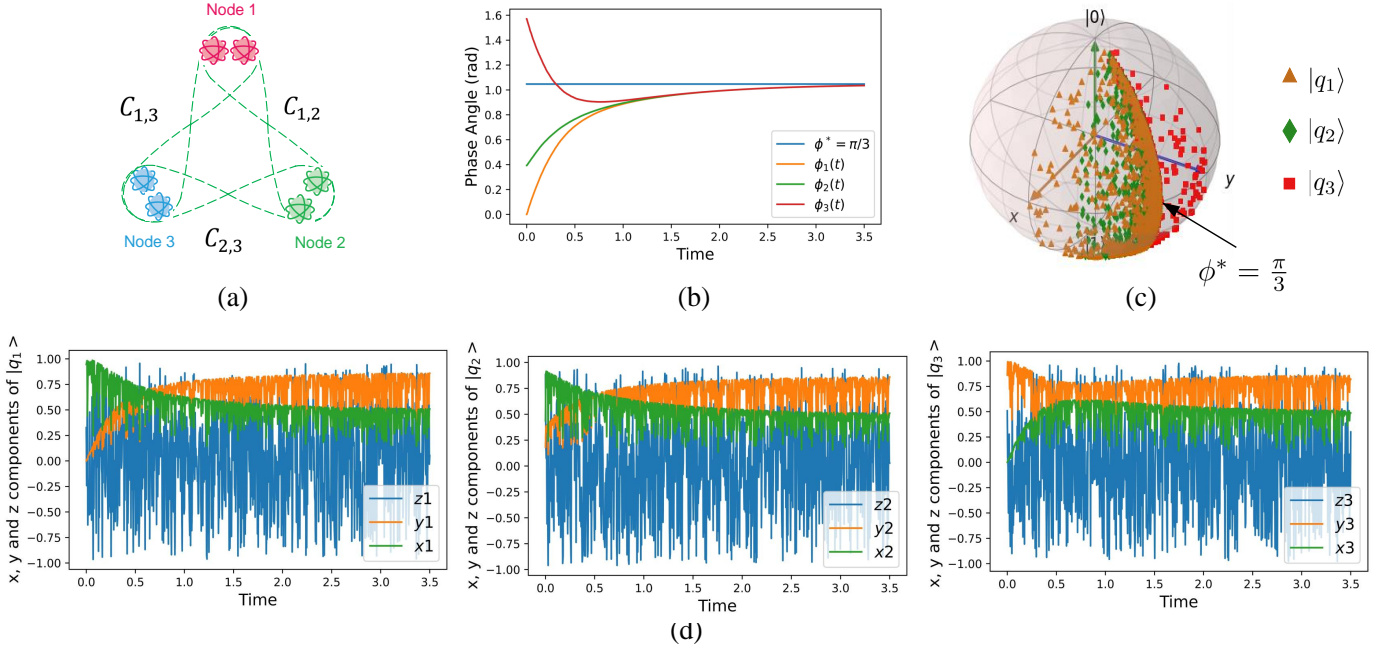


Fig. 4. (a) Connected network of three quantum nodes. (b) Exponential synchronization of phase angles to $\phi^* = \pi/3$. (c) Bloch sphere representation of the states of the quantum nodes along the time. It shows how the additional random θ_i randomizes the states. (d) Measurement outcomes for x, y and z components are random values.

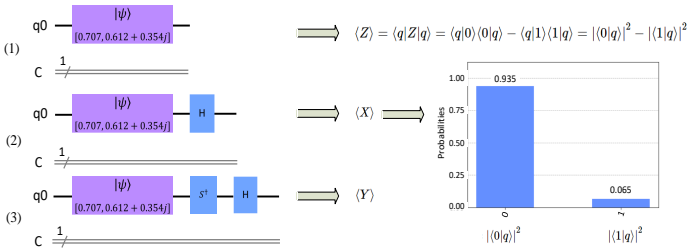


Fig. 5. Measuring the Z basis of the above circuits gives the X, Y and Z components of an arbitrary qubit. The histogram on the right shows the probability of finding the qubit in 0/1 basis with the circuit (2) which is the average over 2000 experiments. Subtracting these two probabilities gives the X component.

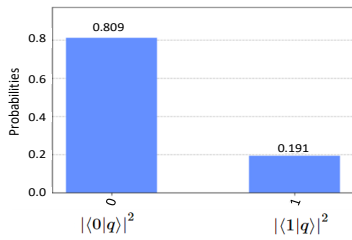


Fig. 6. Measurement result of circuit (2) with randomized θ .

developed quantum distributed controller at the secondary level is formulated as follows:

$$\begin{aligned} \omega_i &= \omega^* - n_i P_i + \frac{\phi_i}{k}, \\ \dot{\phi}_i &= \sin(kn_i P_i - \phi_i) + \sum_{j=1}^n a'_{i,j} \sin(\phi_j - \phi_i), \end{aligned} \quad (21)$$

where ϕ_i/k is the secondary control variable and the scaled power sharing signal, $kn_i P_i$, is the pinner. The power sharing signal is scaled to be restricted to $(0, \pi/2)$ through selecting k such that $k < \frac{\pi/2}{\max(n_i P_i)}$.

At the steady state, the microgrid is assumed stable. Since the DERs' frequency must be equal, we have $\omega_i = \omega_j$ and thus $n_i P_i - \phi_i/k = n_j P_j - \phi_j/k \quad \forall i, j$. As shown before, ϕ_i converges to the pinner as $t \rightarrow \infty$. Thus, $n_i P_i = \phi_i/k$ and $n_i P_i = n_j P_j \quad \forall i, j$ and ω_i converges to ω^* .

• Verification on an AC Networked-Microgrid Case Study

The performance of the developed QSDC is tested on a networked microgrids with five AC microgrids each one has 3 DERs (see Fig. 7). The nominal voltage and frequency are 380 V and 60 Hz respectively. All other parameters can be found in [25]. For the sake of simulation, three scenarios are examined. First, the controller is evaluated in the face of a step load. To verify the controller's feature of plug-and-play capability, as the second scenario, plug-and-play of DERs is tested. Finally, QSDC is tested when some qubits become mixed.

1) *Controller Performance*: Studies in this section illustrate the performance of the QSDC under a step load change of 40 kW applied to microgrid 2 at $t = 10$ s and results are depicted in Fig. 8. The exploited communication graph is shown in Fig. 7. Furthermore, to demonstrate the capability of the controller in handling non-constant droop coefficients, droops at DER₁ and DER₇ change from 5×10^{-3} to 4.7×10^{-3} and from 2×10^{-3} to 2.1×10^{-3} at $t = 17$ s and $t = 20$ s, respectively.

As can be seen, frequency regulation is maintained throughout the step load change and Active power is accurately shared among the heterogeneous DERs throughout the entire runtime. Also, despite changing the droop coefficients, the convergence point of all the power sharing signals, $n_i P_i$, doesn't change as

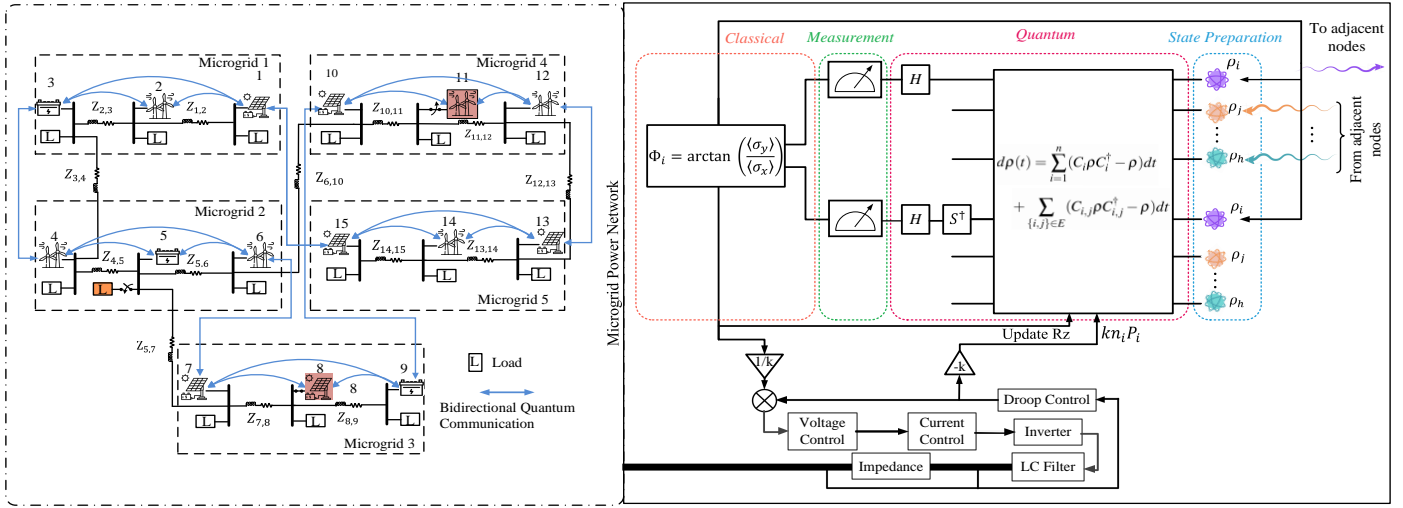


Fig. 7. The AC Networked microgrids case study is shown on the left. Blue bidirectional arrows represent the undirected quantum communications - The figure on the right demonstrates how QSDC is implemented as the secondary controller.

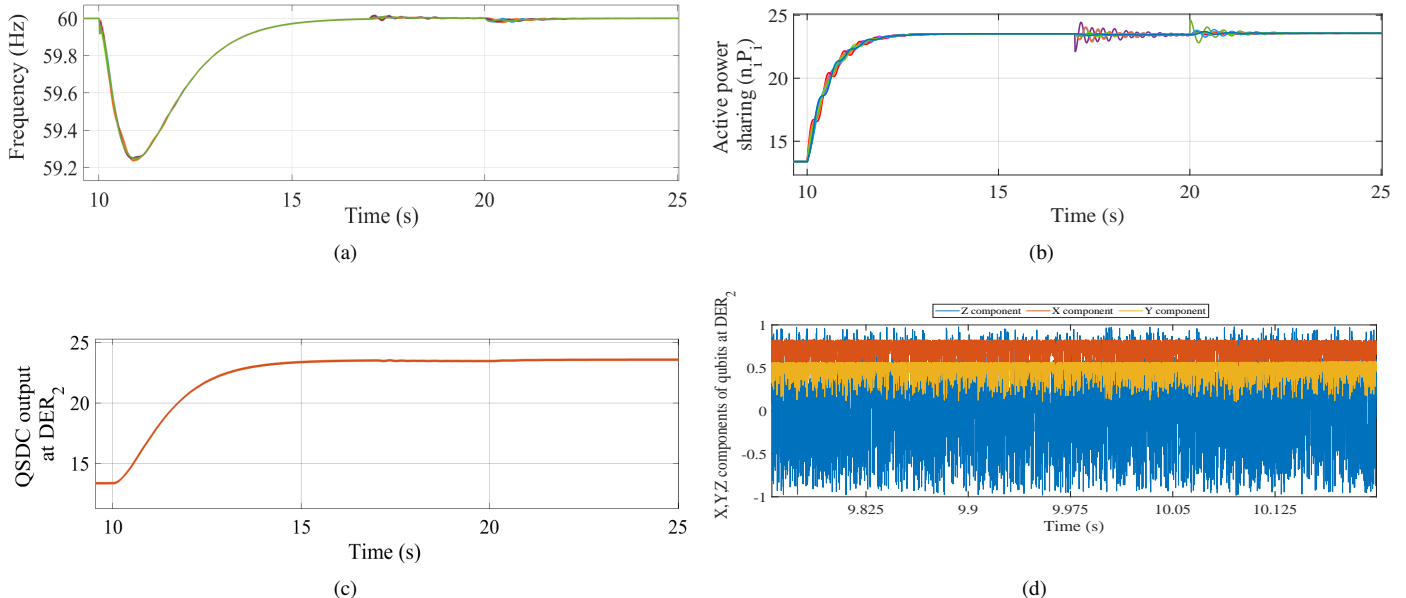


Fig. 8. (a) System's frequency throughout the network after attaching the step load at $t = 10s$ and changing n_1 and n_7 at $t = 17s$ and $t = 20s$, respectively. (b) Active power sharing - all $n_i P_i$ s converge to the same value. (c) QSDC's output at DER_2 . (d) x, y and z components of the qubits at DER_2 .

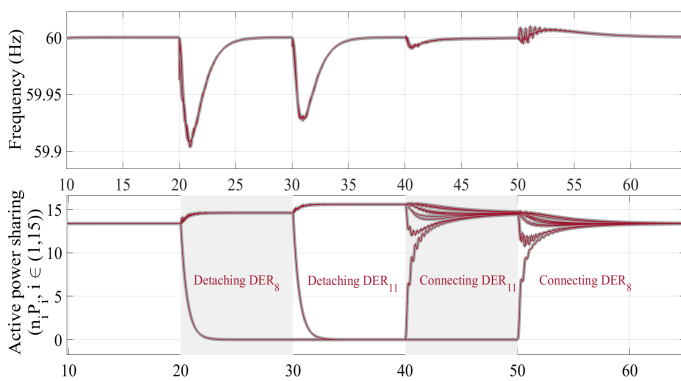


Fig. 9. Performance of QSDC (gray dash line) and DAPI (red dash line) - Frequency regulation and active power sharing after plug-and-play of DER_8 and DER_{11} - At $t = 20s$ and $t = 30s$ the total load is shared among the remaining DERs so their share in power production are increased.

it depends on the power imbalance (power deficiency in this case) at the whole system and not the droop coefficients.

Furthermore, Fig. 8d depicts the randomness of the x, y and z components of the qubits at DER_2 during a short period around $t = 10s$.

2) *Plug-and-play functionality*: As the plug-and-play scenario, DER_8 and DER_{11} are disconnected at $t = 20s$ and $t = 30s$, respectively. Then DER_{11} is reconnected at $t = 40s$ followed by the reconnection of DER_8 at $t = 50s$. Fig. 9 shows how after disconnection of DERs, frequency is regulated to the rated 60 Hz. After disconnection, the active power is shared among the connected DERs, and then re-shared again among all the DERs after DER_8 and DER_{11} are reconnected.

To compare with a classical scheme, Fig. (9) also shows the performance of the distributed-averaging PI (DAPI) controller [32] under the same plug-and-play scenario. As can be

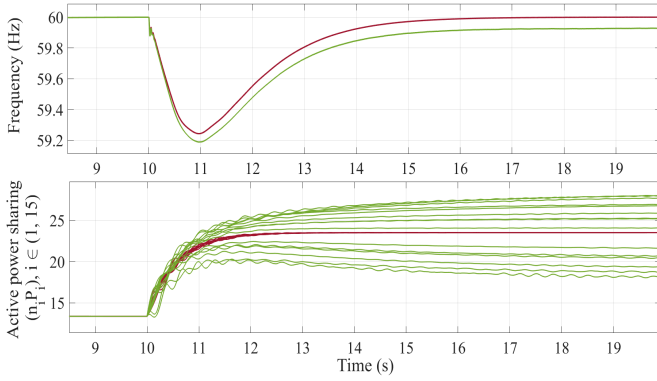


Fig. 10. Performance of QSDC (red solid lines) and QDC (green solid lines) under mixed states condition - With QSDC, frequency is regulated to the 60 Hz and all $n_i P_i$ converge to the same value while, with QDC, frequency regulation and power sharing cannot be guaranteed.

seen, other than providing quantum security on the exchanged information among the participating DERs, the QSDC can guarantee precise power sharing and frequency regulation within a reasonable restoring time compared to the classical solution.

3) *Robustness against mixed states*: Here, we aim to demonstrate that QSDC can handle the problem of mixed states while, under QDC [25], active power sharing and frequency regulation cannot be attained. For this case, the scenario 1) is repeated for when after $t = 10$ s, qubits at DERs 1, 5, 9 and 11 become mixed after master equation evolution. Fig. (10) shows that the performance of the QSDC remains intact (red solid lines) while, with QDC (green solid lines), frequency cannot be regulated to the rated 60 Hz and power sharing is not achieved due to excessive exhaustion of some participating DERs over time.

B. DC Microgrids

In DC microgrids, droop control function is mainly utilized to provide decentralized power sharing. It generates the voltage reference V_i^{ref} as $V_i^{\text{ref}} = V^* - m_i I_i$ [33], where V^* is the nominal dc voltage, m_i is the current droop gain and I_i is the output current of DER $_i$. Consider the DC microgrid depicted in Fig. (11), ignoring the inductance effect of lines, the DC bus voltage V_b can be determined as $V_b = V_i^{\text{ref}} - R_i I_i$.

It can be shown that, if the current droop gain m_i is set much larger than the line resistance R_i , $\frac{I_i}{I_j} \approx \frac{m_i}{m_j}$ and $V_b \approx V_i^{\text{ref}} \forall i, j$. The larger m_i is chosen, the more accurate power sharing can be obtained; however, larger m_i may cause the dc bus voltage V_b to deviate more from the nominal value V^* . Therefore, we aim to attain power sharing and voltage restoration simultaneously, by adding the QSDC. To equip the DC microgrid with the QSDC, the droop function is modified as

$$\begin{aligned} V_i^{\text{ref}} &= V^* - m_i I_i + \frac{\phi_i}{c}, \\ \dot{\phi}_i &= \sin(cm_i I_i - \phi_i) + \sum_{j=1}^n a_{i,j} \sin(\phi_j - \phi_i), \end{aligned} \quad (22)$$

Again, we select c such that $c < \frac{\pi/2}{\max(m_i I_i)}$. Obviously, the first part in the secondary control dynamic is to drive the dc bus voltage V_b to the nominal value V^* while the second part is to guarantee that $\phi_i = \phi_j$ is satisfied, i.e., the current sharing is

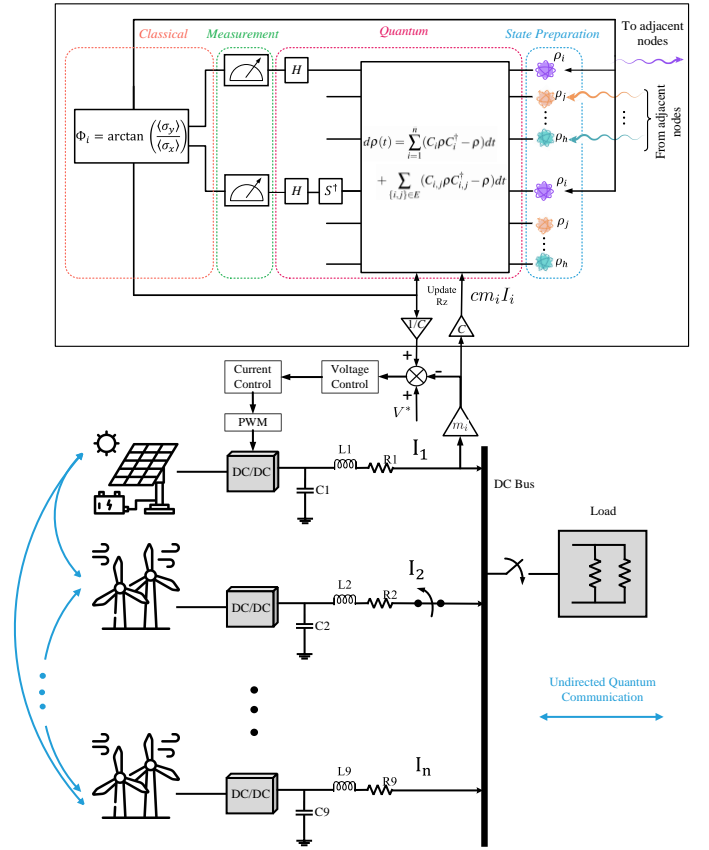


Fig. 11. DC microgrid model equipped with the QSDC.

achieved which demonstrates that the QSDC is also applicable to distributed voltage control in DC microgrids.

• Verification on a DC Microgrid Case Study

To demonstrate the universality of the QSDC, a 9-DER DC microgrid case study [25] is equipped with QSDC (see Fig. 11). It is assumed that qubits at DERs 2, 3 and 5 become mixed after $t = 20$ s. First, a step load $R_L = 3\Omega$ is applied at $t = 20$ s. Results are depicted in Fig. (12a). The exploited communication graph is shown in Fig. (11). As can be seen, voltage regulation is guaranteed throughout the step load disturbance. Then, to verify the plug-and-play functionality, at $t = 28$ s DER $_2$ is disconnected and attached again at $t = 35$ s. Fig. (12a) shows how the current (power) is shared among the participating DERs while voltage regulation is preserved along the time.

To compare with QDC, the same scenario is repeated for when the microgrid is working under QDC and results are demonstrated in Fig. (12b). As shown, the problem of mixed states prevents the QDC from guaranteeing voltage regulation and current sharing.

IV. CONCLUSION

Resilience of the current schemes on classical communication makes microgrids vulnerable to cyber attacks. Inspired by quantum properties of quantum bits, in this paper, we devise a scalable quantum-secure distributed controller that can guarantee synchronization and power sharing among participating DERs. We show that in the developed scheme, by allocating random θ angle to the qubits at the initialization step at each node, the

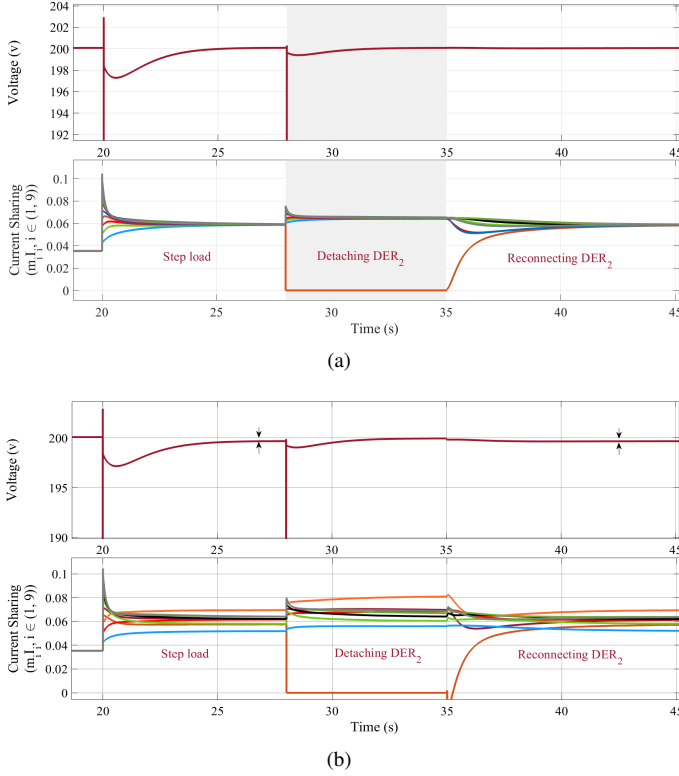


Fig. 12. (a) Voltage regulation and current sharing after a step load disturbance and plug-and-play of DER₂, under mixed states condition. (b) Performance of QDC under mixed states situation - Voltage regulation and current sharing cannot be guaranteed.

security of the protocol can be unprecedentedly enhanced since, the measurement outcomes of the exchanged qubits, obtained by a third-party agent, would be some random values which do not reveal meaningful information. The new quantum distributed control scheme thus assures provably cyber-resilient microgrids.

APPENDIX A PRELIMINARIES

1) *Graph Theory*: A simple graph $G = (V, E)$ consists of a set of n nodes, $V = \{v_1, v_2, \dots, v_n\}$, and a set of edges, $E \subset V \times V$. An edge $(v_i, v_j) \in E$ represents that nodes v_i and v_j can exchange information with each other. A sequence of non-repeated edges $(v_i, v_{p_1}), (v_{p_1}, v_{p_2}), \dots, (v_{p_{m-1}}, v_{p_m}), (v_{p_m}, v_j)$ is called a path between nodes v_i and v_j . If there exists a path between any two different nodes $v_i, v_j \in V$, G is called connected. A node v_j is called a neighbor of node v_i if $(v_j, v_i) \in E$. The set of neighbors of node v_i is denoted as $N_i = \{v_j \in V \mid (v_j, v_i) \in E\}$. The adjacency matrix of graph G , denoted as A , is an $n \times n$ matrix whose entries $a_{i,j} = 1$ if $v_j \in N_i$ and $a_{i,j} = 0$ otherwise. The degree matrix D of graph G , denoted as D , is defined as an $n \times n$ diagonal matrix whose i th diagonal entry equals the degree of node v_i , i.e., $\sum_{v_j \in N_i} a_{i,j}$. The Laplacian matrix of graph G , denoted as L , is defined as $D - A$. Note that A, D, L are all symmetric. The node-edge incidence matrix $B \in R^{V \times E}$ is defined component-wise as $B_{i,j} = 1$ if edge j enters node i , $B_{i,j} = -1$ if edge j leaves node i , and $B_{i,j} = 0$ otherwise. For $x \in R^V$, $B^T x \in R^E$ is the vector with components $x_i - x_j$, with $\{i, j\} \in E$. If $\text{diag}(\{a_{i,j}\}_{\{i,j\} \in E})$ is the diagonal matrix of edge weights, then the Laplacian matrix is given by $L = B \text{diag}(\{a_{i,j}\}_{\{i,j\} \in E}) B^T$.

2) *Quantum Systems and Notations*: The (adjoint) \dagger symbol indicates the transpose-conjugate in matrix representation, and the tensor product \otimes is associated to the Kronecker product.

The mathematical description of a single quantum system starts by considering a complex Hilbert space \mathcal{H} . We utilize Dirac's notation, where $|\psi\rangle$ denotes an element of \mathcal{H} , called a ket which is represented by a column vector, while $\langle\psi| = |\psi\rangle^\dagger$ is used for its dual, a bra, represented by a row vector, and $\langle\psi|\varphi\rangle$ for the associated inner product. We denote the set of linear operators on \mathcal{H} by $\mathfrak{B}(\mathcal{H})$. The adjoint operator $X^\dagger \in \mathfrak{B}(\mathcal{H})$ of an operator $X \in \mathfrak{B}(\mathcal{H})$ is the unique operator that satisfies $(X|\psi\rangle)^\dagger|\chi\rangle = \langle\psi|(X^\dagger|\chi\rangle)$ for all $|\psi\rangle, |\chi\rangle \in \mathcal{H}$. The natural inner product in $\mathfrak{B}(\mathcal{H})$ is the Hilbert-Schmidt product $\langle X, Y \rangle = \text{tr}(X^\dagger Y)$, where tr is the usual trace functional which is canonically defined in a finite dimensional setting. We denote by I the identity operator. $[A, B] = AB - BA$ is the commutator and $\{A, B\} = AB + BA$ is the anticommutator of A and B .

Qubit, defined as the quantum state of a two-state quantum system, is the smallest unit of information, and it is analogous to classical bit. State of a qubit, represented by $|\psi\rangle = \alpha|0\rangle + \beta|1\rangle$, is superposition of the two orthogonal basis states $|0\rangle \sim [1, 0]^T$ and $|1\rangle \sim [0, 1]^T$. α and β are complex numbers in general, where $|\alpha|^2 + |\beta|^2 = 1$. We denote $|q_1\rangle \otimes \dots \otimes |q_n\rangle \in \mathcal{H}^{\otimes n}$ as $|q_1 \dots q_n\rangle$ where \otimes represents the tensor product. Since $|\alpha|^2 + |\beta|^2 = 1$, we can represent the state of a qubit by $|\psi\rangle = \cos \frac{\theta}{2} |0\rangle + e^{i\phi} \sin \frac{\theta}{2} |1\rangle$ where θ and ϕ are real numbers defining a point on a unit three-dimensional sphere called Bloch sphere.

In the case of mixed state, the state of a quantum system is represented by a *density operator* ρ , that is any self-adjoint positive semi-definite operator with trace one, and $\rho = |\psi\rangle\langle\psi|$ with $|\psi\rangle \in \mathcal{H}$ and $\langle\psi|\psi\rangle = 1$ are called pure states. For further information on qubits see [27], [29].

APPENDIX B PROOF OF CONVERGENCE FOR EQ. (17)

For synchronization of the system, it is critical that the pinner for all of the oscillators be the same, i.e., $\phi_{t,i} = \phi^*$, otherwise, synchronization cannot be achieved in general. To study whether quantum node i is synchronized to the pinner, it is convenient to study the phase deviation of quantum node i from the pinner. We introduce the following change of variables,

$$\phi_i = \phi^* + \zeta_i, \quad (23)$$

where ζ_i denotes the phase deviation of the i th oscillator from the pinner ϕ^* . Substituting (23) into (16), we have

$$\dot{\zeta}_i = \sum_{j=1}^n a'_{i,j} \sin(\zeta_j - \zeta_i) - \sin(\zeta_i). \quad (24)$$

By studying the properties of (24), we can obtain the condition for synchronization. If all ζ_i 's converge to 0, then we have $\phi_i = \phi^*$ as $t \rightarrow \infty$, indicating that all nodes are synchronized to the pinner. Let $B = [B_{i,j}]_{n \times m}$ be the incidence matrix [34] of the communication graph G with m being the number of edges. Then, (24) can be recast in a state form:

$$\dot{\zeta} = -\sin \zeta - BW \sin(B^T \zeta), \quad (25)$$

where $W = \text{diag}(\{a'_{i,j}\}_{\{i,j\} \in E})$ is the diagonal matrix of edge weights and $\sin(\cdot)$ takes entry-wise operation for a vector.

To proceed, set $\varepsilon = \max_{1 \leq i \leq n} |\zeta_i|$. When $\varepsilon < (\pi/2)$, if $\zeta_i = \varepsilon$, we have $-\pi < -2\varepsilon \leq \zeta_j - \zeta_i \leq 0$ for $1 \leq j \leq n$. Hence, in (24), $\sin(\zeta_j - \zeta_i) \leq 0$ and $\sin \zeta_i > 0$ hold, and hence $\dot{\zeta}_i < 0$ hold. Therefore, the vector field is pointing inward in the set, and no trajectory can escape to values larger than ε . Similarly, it can be obtained that, when $\zeta_i = -\varepsilon$, $\dot{\zeta}_i > 0$ holds. Thus no trajectory can escape to values smaller than $-\varepsilon$. Therefore, $\zeta \in [-\varepsilon, \varepsilon] \times \cdots \times [-\varepsilon, \varepsilon] = [-\varepsilon, \varepsilon]^n$ is positively invariant when $\varepsilon < \pi/2$, where \times denotes Cartesian product. Define a Lyapunov function $V = (1/2)\zeta^T \zeta$, which equals zero only if all ζ_i are zero, meaning the synchronization of all nodes to the pinner. Differentiating V along the trajectories of (25) yields

$$\dot{V} = -\zeta^T S_1 \zeta - \zeta^T B W S_2 B^T \zeta, \quad (26)$$

where $S_1 \in R^{n \times n}$ and $S_2 \in R^{m \times m}$ are given by

$$\begin{aligned} S_1 &= \text{diag} \{ \text{sinc}(\zeta_1), \dots, \text{sinc}(\zeta_n) \}, \\ S_2 &= \text{diag} \{ \text{sinc}(B^T \zeta)_1, \dots, \text{sinc}(B^T \zeta)_m \}, \end{aligned} \quad (27)$$

where $\text{sinc}(x) \equiv \sin(x)/x$ and $(B^T \zeta)_i$ denotes the i th element of m -dimensional vector $B^T \zeta$. When all ζ_i are within $[-\varepsilon, \varepsilon]$ with $0 \leq \varepsilon < (\pi/2)$, $(B^T \zeta)_i$ is in the form of $\zeta_k - \zeta_l$ ($1 \leq k, l \leq n$), and hence is restricted to $(-\pi, \pi)$. Given that in $(-\pi, \pi)$, $\text{sinc}(x) > 0$ holds, it follows that $S_1 \geq \sigma_1 I$ and $S_2 \geq \sigma_2 I$ with $\sigma_1 = \text{sinc}(\varepsilon)$ and $\sigma_2 = \text{sinc}(2\varepsilon)$. Thus, $S_1 + B W S_2 B^T \geq \sigma_1 I + \sigma_2 B W B^T$, which in combination with (26) yields $\dot{V} \leq -\zeta^T (\sigma_1 I + \sigma_2 B W B^T) \zeta$. Note that $B W B^T$ is the Laplacian matrix of the underlying graph G , which is always positive semidefinite. Since σ_1 and σ_2 are positive,

$\sigma_1 I + \sigma_2 B W B^T$ must be positive definite. It follows that, when $0 \leq \varepsilon < (\pi/2)$, we have $\dot{V} \leq -2\mu V$, where $\mu = \lambda_{\min}(\sigma_1 I + \sigma_2 B W B^T) > 0$, which implies that all the nodes will synchronize to the pinner exponentially fast at a rate no less than μ , which is dependent on the network connectivity.

REFERENCES

- [1] Thomas Morstyn, Niall Farrell, Sarah J. Darby, and Malcolm D. McCulloch, "Using peer-to-peer energy-trading platforms to incentivize prosumers to form federated power plants," *Nature Energy*, vol. 3, no. 2, pp. 94–101, 2018.
- [2] Pouya Babahajiani, Lizhi Wang, Ji Liu, and Peng Zhang, "Push-Sum-Enabled Resilient Microgrid Control," *IEEE Trans. Smart Grid*, vol. 12, no. 4, pp. 3661–3664, 2021.
- [3] Mahdiah S. Sadabadi, Subham Sahoo, and Frede Blaabjerg, "A Fully Resilient Cyber-Secure Synchronization Strategy for AC Microgrids," *IEEE Trans. Power Electron.*, vol. 36, no. 12, pp. 13372–13378, 2021.
- [4] Q. Zhou, M. Shahidehpour, A. Alabdulwahab, and A. Abusorrah, "A Cyber-Attack Resilient Distributed Control Strategy in Islanded Microgrids," *IEEE Trans. Smart Grid*, vol. 11, no. 5, pp. 3690–3701, 2020.
- [5] S. Sahoo, T. Dragičević, and F. Blaabjerg, "Multilayer Resilience Paradigm Against Cyber Attacks in DC Microgrids," *IEEE Trans. Power Electron.*, vol. 36, no. 3, pp. 2522–2532, 2021.
- [6] Y. Chen, D. Qi, H. Dong, C. Li, Z. Li, and J. Zhang, "A FDI Attack-Resilient Distributed Secondary Control Strategy for Islanded Microgrids," *IEEE Trans. Smart Grid*, vol. 12, no. 3, pp. 1929–1938, 2021.
- [7] S. Sahoo, Y. Yang, and F. Blaabjerg, "Resilient Synchronization Strategy for AC Microgrids Under Cyber Attacks," *IEEE Trans. Power Electron.*, vol. 36, no. 1, pp. 73–77, 2021.
- [8] K. Wright, K.M. Beck, S. Debnath, J.M. Amini, Y. Nam, N. Grzesiak, J.-S. Chen, N.C. Pistenti, M. Chmielewski, C. Collins, et al., "Benchmarking an 11-Qubit Quantum Computer," *Nature Communications*, vol. 10, no. 1, pp. 1–6, 2019.
- [9] R. Qi, Z. Sun, Z. Lin, P. Niu, W. Hao, L. Song, Q. Huang, J. Gao, L. Yin, and G.-L. Long, "Implementation and Security Analysis of Practical Quantum Secure Direct Communication," *Light: Science & Applications*, vol. 8, no. 1, pp. 1–8, 2019.
- [10] D. Awschalom, K.K. Berggren, H. Bernien, S. Bhave, L.D. Carr, P. Davids, S.E. Economou, D. Englund, A. Faraon, M. Fejer, et al., "Development of Quantum Interconnects (QuICs) for Next-Generation Information Technologies," *PRX Quantum*, vol. 2, no. 1, pp. 017002, 2021.
- [11] G. Popkin, "The Internet Goes Quantum," *Science*, vol. 372, no. 6546, pp. 1026–1029, 2021.
- [12] Y. Yu, F. Ma, X.-Y. Luo, B. Jing, P.-F. Sun, R.-Z. Fang, C.-W. Yang, H. Liu, M.-Y. Zheng, X.-P. Xie, et al., "Entanglement of Two Quantum Memories via Fibres Over Dozens of Kilometres," *Nature*, vol. 578, no. 7794, pp. 240–245, 2020.
- [13] D. Castelvecchi, "Quantum Network is Step Towards Ultrasecure Internet," *Nature*, vol. 590, no. 7847, pp. 540–541, 2021.
- [14] Y.-A. Chen, Q. Zhang, T.-Y. Chen, W.-Q. Cai, S.-K. Liao, J. Zhang, K. Chen, J. Yin, J.-G. Ren, Z. Chen, et al., "An Integrated Space-to-Ground Quantum Communication Network Over 4,600 Kilometres," *Nature*, vol. 589, no. 7841, pp. 214–219, 2021.
- [15] Y.-H. Luo, H.-S. Zhong, M. Erhard, X.-L. Wang, L.-C. Peng, M. Krenn, X. Jiang, L. Li, N.-L. Liu, C.-Y. Lu, et al., "Quantum Teleportation in High Dimensions," *Physical Review Letters*, vol. 123, no. 7, pp. 070505, 2019.
- [16] Z. Qi, Y. Li, Y. Huang, J. Feng, Y. Zheng, and X. Chen, "A 15-User Quantum Secure Direct Communication Network," *Light: Science & Applications*, vol. 10, no. 1, pp. 1–8, 2021.
- [17] J.-Y. Hu, B. Yu, M.-Y. Jing, L.-T. Xiao, S.-T. Jia, G.-Q. Qin, and G.-L. Long, "Experimental Quantum Secure Direct Communication with Single Photons," *Light: Science & Applications*, vol. 5, no. 9, pp. e16144, 2016.
- [18] S. Pirandola, S. Mancini, S. Lloyd, and S.L. Braunstein, "Continuous-Variable Quantum Cryptography Using Two-Way Quantum Communication," *Nature Physics*, vol. 4, no. 9, pp. 726–730, 2008.
- [19] S.K. Joshi, D. Aktas, S. Wengerowsky, M. Lončarić, S.P. Neumann, B. Liu, T. Scheidl, G.C. Lorenzo, Ž. Samec, L. Kling, et al., "A Trusted Node-Free Eight-User Metropolitan Quantum Communication Network," *Science Advances*, vol. 6, no. 36, pp. eaba0959, 2020.
- [20] L. Mazzarella, A. Sarlette, and F. Ticozzi, "Consensus for Quantum Networks: Symmetry From Gossip Interactions," *IEEE Trans. Autom. Control*, vol. 60, no. 1, pp. 158–172, 2015.
- [21] Luca Mazzarella, Francesco Ticozzi, and Alain Sarlette, "Extending robustness and randomization from consensus to symmetrization algorithms," *SIAM Journal on Control and Optimization*, vol. 53, no. 4, pp. 2076–2099, 2015.
- [22] G. Shi, D. Dong, I. R. Petersen, and K. H. Johansson, "Reaching a Quantum Consensus: Master Equations That Generate Symmetrization and Synchronization," *IEEE Transactions on Automatic Control*, vol. 61, no. 2, pp. 374–387, 2016.
- [23] Heinz-Peter Breuer and Francesco Petruccione, *The Theory of Open Quantum Systems: 1st Edition*. Oxford, U.K.: Oxford University Press, 2002.
- [24] G. Lindblad, "On the generators of quantum dynamical semigroups," *Communications in Mathematical Physics*, vol. 48, no. 2, pp. 119–130, 1976.
- [25] Pouya Babahajiani, Peng Zhang, Tzu-Chieh Wei, Ji Liu, and Xiaonan Lu, "Employing Interacting Qubits for Distributed Microgrid Control," *IEEE Transactions on Power Systems*, pp. 1–13, 2022.
- [26] Howard M. Wiseman and Gerard J. Milburn, *Quantum Measurement and Control*. Cambridge, U.K.: Cambridge University Press, 2009.
- [27] J. Preskill, *Lecture Notes for Physics: Quantum Information and Computation*. Pasadena, CA, USA: California Institute of Technology, 1998.
- [28] Chris Godsil and Gordon Royle, *Algebraic Graph Theory*. New York, NY, USA: Springer-Verlag, 2001.
- [29] Michael A. Nielsen and Isaac L. Chuang, *Quantum Computation and Quantum Information*. Cambridge, U.K.: Cambridge University Press, 2010.
- [30] Giacomo Torlai, Guglielmo Mazzola, Juan Carrasquilla, Matthias Troyer, Roger Melko, and Giuseppe Carleo, "Neural-network quantum state tomography," *Nature Physics*, vol. 14, no. 5, pp. 447–450, 2018.
- [31] J.R. Johansson, P.D. Nation, and Franco Nori, "QuTiP 2: A Python framework for the dynamics of open quantum systems," *Computer Physics Communications*, vol. 184, no. 4, pp. 1234–1240, 2013.
- [32] John W. Simpson-Porco, Qobad Shafiee, Florian Dörfler, Juan C. Vasquez, Josep M. Guerrero, and Francesco Bullo, "Secondary Frequency and Voltage Control of Islanded Microgrids via Distributed Averaging," *IEEE Transactions on Industrial Electronics*, vol. 62, no. 11, pp. 7025–7038, 2015.
- [33] Vahidreza Nasirian, Ali Davoudi, Frank L. Lewis, and Josep M. Guerrero, "Distributed Adaptive Droop Control for DC Distribution Systems," *IEEE Transactions on Energy Conversion*, vol. 29, no. 4, pp. 944–956, 2014.
- [34] Chris Godsil and Gordon Royle, *Algebraic Graph Theory*. New York, NY, USA: Springer-Verlag, 2001.